STUDY ON THE THERMAL RESPONSE OF SPIRAL ENERGY PILES BASED ON FIELD TEST

Hong CHANG [*], Haoquan WANG, Fengquan SHEN, Wanli ZHU

[*1] School of geomatics and prospecting engineering, Jilin Jianzhu University, Changchun 130118, China

[*] Corresponding author; E-mail: changhong0431@163.com; Tel.: +86-1319-600-1641

Abstract: *Field tests of spiral energy piles under the combined effect of temperature and loading are relatively few. Based on the field test, the heat transfer efficiency, pile strain, axial force and shaft friction of two spiral energy piles were studied. The major findings of the experimental studies were as follows: First, when the double spiral energy pile was heated, the temperature distribution was more uniform; the total heat transfer and the heat transfer rate were higher than those of the single spiral energy pile. Second, the pile strain distribution was such that smaller values were noticed at both pile ends while larger values were in the middle part of the pile. The additional tensile stresses of the two piles generated during cooling reached 4.06 MPa and 4.75 MPa, which exceeded the tensile strength of concrete. Finally, during heating, the shaft friction was negative in the middle and upper pile and positive in the middle and lower pile. The single spiral energy pile showed two neutral points. The downward load generated by the single spiral energy pile was about 885 kN higher than that generated by the double one. The above changes should be focused on in the actual project.*

Keywords*: energy pile; spiral type; field test; thermal response; temperature and loading effect*

1. Introduction

As a sustainable and clean geothermal resource, shallow geothermal energy is widely used in ground source heat pump technology. The traditional ground source heat pump technology is less applied in China due to its high drilling cost and large land occupation. In contrast, the energy pile has high heat transfer efficiency and good bearing capacity and also saves land area. Thus, it is widely used in construction engineering worldwide. The form of energy pile buried pipe has developed from the initial single U-shaped to double U-shaped, W-shaped, spiral-shaped [1], deeply penetrating U-shaped heat exchanger [2], etc.

A considerable amount of literature has been published on energy piles. Morino et al. [3] first proposed a buried tube heat exchanger based on the pile. The heat transfer between the pile and the soil was realized by the water cycle in the steel pile. They studied the quantity of heat exchanged with the soil and water temperature variations in the steel pile. Based on the finite line-source theory, Yi et al. [4] presented an analytical solution of soil temperature variation in the radial and depth directions of the cylindrical heat source model by Green's function method. The research has

been deepened on the heat transfer performance of energy piles with different buried pipe forms. Aks et al. [5] compared and analyzed the thermal interaction of different buried pipelines, such as U-shaped, double U-shaped, W-shaped, and 3-U-shaped pipes in series, 3-U-shaped pipes in parallel, and spiral-shaped pipes. The results showed that thermal interaction between the inlet and outlet pipes was significantly affected by the number of loops, position of pipes, and the thermal conductivity of the surrounding soil and concrete. Wu et al. [6] buried single and double U-shaped pipes in prestressed high-strength concrete (PHC) piles and monitored their temperature and strain using distributed fiber optic sensing technology. The heat transfer efficiency of PHC energy piles was inefficient throughout the process. Thus, they suggested further research on the buried pipe method and pile core backfill to improve the heat transfer efficiency of energy piles. The use of energy piles is also becoming increasingly important in engineering practice. Lu et al. [7] performed field tests on the thermal response characteristics and the stress of the raft affected by the energy pile in the pile-raft foundation. By monitoring the variation in pile temperature, pile stress, and raft stress, they found certain tensile stress on the upper edge of the raft during heating of the energy piles without load constraint. Lv et al. [8] conducted field tests on the axial and radial thermal responses of friction-type energy piles in clay. They monitored the thermodynamic parameters, such as inlet and outlet temperature, pile temperature, and strain, and compared the friction-type energy piles in dense sand. It was concluded that the radial thermal stress of piles was much lower than the axial thermal stress. As the axial constraint increased, the axial thermal stress of the energy pile in clay also increased. To improve the heat transfer effect, bearing capacity, and thermal storage properties of energy piles, many scholars [9-11] have started to prepare innovative high-performance concrete as pile materials.

At present, most studies are limited to the indoor model test [12-14] and numerical simulation [15, 16], and the field test study of energy piles is scarce. The spiral-shaped pipe is characterized by a large heat transfer range and high heat transfer efficiency. However, since the economic cost is expensive [17], and the construction difficulty is greater than that of other buried pipe forms, the engineering application experience for spiral buried pipes remains scarce. Such valuable experience is needed for applying spiral energy piles in practical construction engineering. In this paper, two energy piles, single and double spiral-shaped pipes, were tested under the combined effects of temperature and loading. At a constant heating power of 10 kW, thermodynamic parameters such as circulating water temperature, pile temperature, and steel bar stress were compared to analyze the changes in heat transfer efficiency, strain, axial force, and shaft friction of energy piles. This paper can provide valuable experience for future engineering practice of spiral energy piles.

2. Materials and Methods

2.1. Nature of the soil layer on site

The field test was located in Beihu District, Changchun City, Jilin Province, China. The groundwater level measured at the beginning of the experiment was 2.40–5.50 m. The distribution of soil layers and the physical and mechanical indexes of the soil were obtained through in-situ tests, wave velocity tests, and laboratory soil tests. The specific data are shown in Tab. 1 and Tab. 2.

Table 1. Distribution of soil layers on site

Name of soil layer	Depth (m)	Thickness (m)	Soil state
Miscellaneous soil	0–2.1	2.1	Loose
Plain filling soil	2.1–3.8	1.7	Soft-plastic
Silty clay	3.8–7.4	3.6	Soft-plastic
Gravelly sand	7.4–11.2	3.8	Slightly dense
Mudstone	11.2–25	13.8	Solid

Table 2. Physical and mechanical indexes of soil

Soil layer	Depth (m)	Plasticity index	Liquidity index	Compressibility coefficient (MPa)
Silty clay	5–5.2	13.5	0.59	0.412
Silty clay	6–6.2	13.3	0.25	0.23

Soil layer	Granulometric composition				
Gravelly sand	Gravel 20.0–2.00	Coarse sand 2.00–0.50	Medium sand 0.50–0.25	Fine sand 0.25–0.075	Silty sand 0.075–0.05
Content (%)	33.3	25.5	19.5	18.4	3.3

2.2. Energy pile and sensor placement

The test piles were drilled grouting piles. The heat exchange pipe was fixed in a steel bar cage with steel wires in advance. Then, the cage was pressed into a drill hole filled with concrete, and the heat exchange pipe was extended to the ground. As shown in Fig. 1, the test piles are a single spiral-shaped pipe and a double spiral-shaped pipe. The smaller coil pitch can improve heat transfer efficiency [18], but the tighter configuration of the coil pitch may cause thermal interference between pipes [19]. To reduce energy consumption, the coil pitch was controlled at 300 mm. Figure 2 shows the site installation of the steel bar cage and sensor.

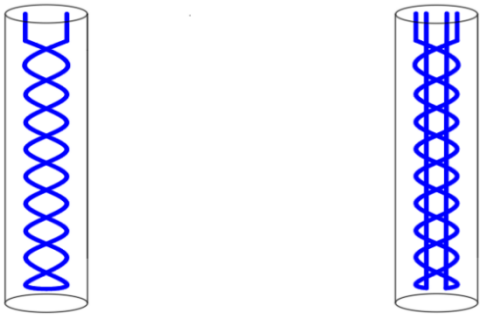

(a) Single spiral energy pile (b) Double spiral energy pile

Figure 1. Schematic diagram of energy piles

(a) Layout of the steel bar cage (b) Sensor installation

Figure 2. Construction of the energy pile

The experiment is divided into two groups. The pile diameter is 800 mm, the effective pile length is 13 m, and the top of the pile is 7.1 m from the outdoor ground. The pile material is C40P8 impermeable concrete. According to the literature [20], the elastic modulus of concrete is 3.25×10^4 N/mm^2, and the thermal expansion coefficient αc is 1.0×10^{-5} ε /℃. The heat exchange pipe is a PE pipe with an outer diameter of 20 mm and a wall thickness of 2 mm. As shown in Fig. 3, seven and six sensors are arranged in the two piles to simultaneously monitor the steel bar stress and pile temperature change. The flow rate of the circulating water pump is 3 m^3/h, and the maximum lift is 35 m. The heating system is a constant temperature heating water tank with a power of 10 kW.

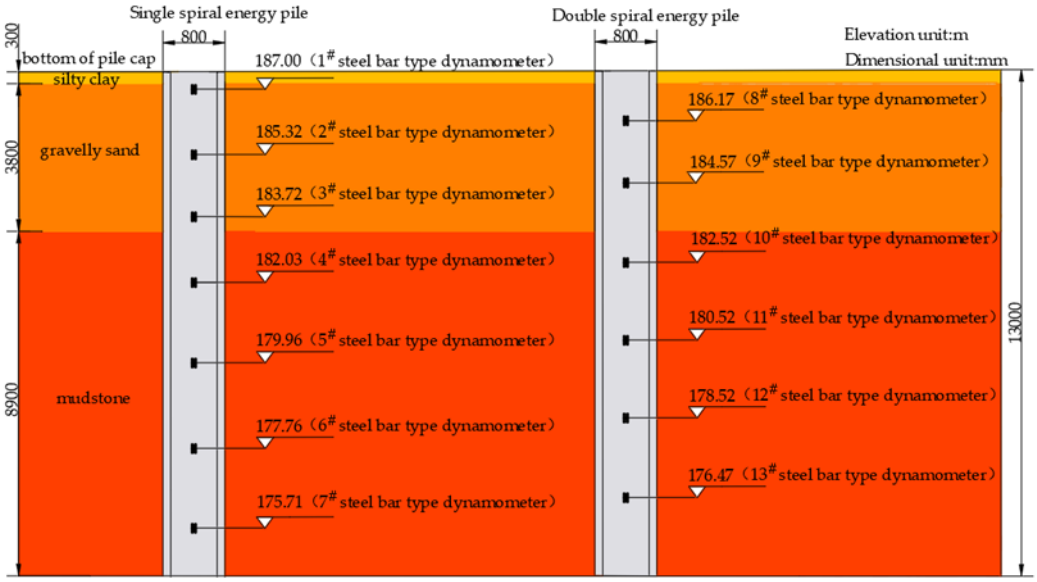

Figure 3. Schematic diagram of the overall experimental setup

2.3. Experimental scheme

The field test began on April 19, 2021, in sunny weather with an average daytime temperature of 19 ℃ and an average nighttime temperature of 5 ℃. The test was divided into two working conditions: cooling and heating. First, the energy pile was circulated at a constant heat power of 10 kW for 56 hours. Then, heating and circulation were stopped, and the pile was cooled naturally for 24 hours. Since the energy piles in this test were in different soil layers, their heat transfer efficiency was

related to the thermal conductivity of the piles, the form of buried pipes and the type of soil. Therefore, in this field test, changes in heat transfer efficiency, strain, axial force, and shaft friction of the two energy piles were investigated by monitoring the field test data such as circulating water temperature, pile temperature, and steel bar stress.

3. Results and Discussion

3.1. Water temperature variation

The variation in circulating water temperature at different moments is shown in Fig. 4. At the beginning of heating, the temperature difference between inlet and outlet water of the single spiral energy pile is stable at about 7–8 ℃, and the heat exchange power is stable at about 9.44 kW. The temperature difference between inlet and outlet water of the double spiral energy pile is stable at about 4–5 ℃, and the heat exchange power is stable at about 9.7 kW. This result shows that at a constant heating power of 10 kW, the two energy piles can quickly reach heat transfer equilibrium, with basically unchanged heat transfer power. When the heating is stopped, the total heat transfer of the double spiral energy pile is higher than that of the single one.

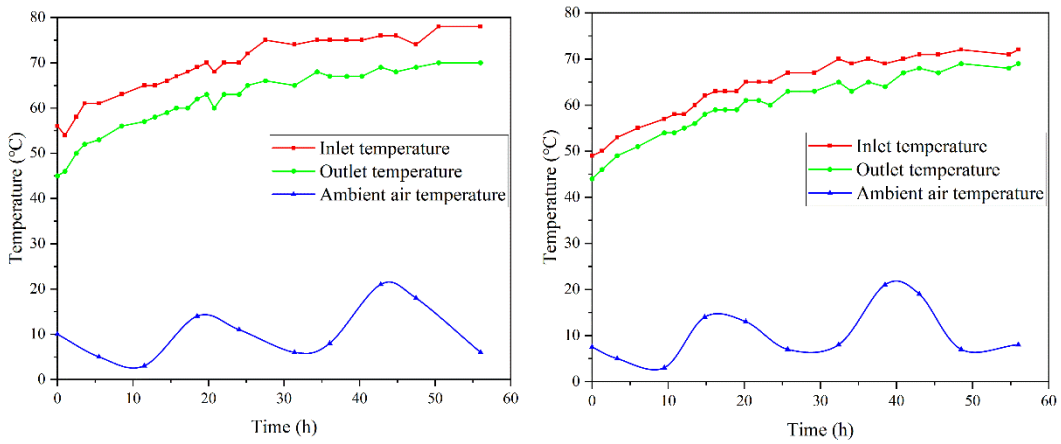

(a) Single spiral energy pile **(b) Double spiral energy pile**

Figure 4. Circulating water temperature and ambient air temperature

3.2. Pile temperature variation

The variation in pile temperature follows the variation pattern of water temperature. During heating, the pile temperature continuously increases. Figure 5(a) shows that the temperature of the single spiral energy pile is discrete within the depth of 0–7.5 m, which does not occur in the double spiral energy pile. The maximum pile temperature difference of the single spiral pile at the beginning of heating is 7 ℃ and increases to 16.8 ℃ at the end. The excessive temperature difference can lead to uneven stress in various pile parts. Therefore, attention should be paid to the influence of discrete temperature distribution on the bearing capacity of piles when applying the single spiral energy pile in practical engineering.

According to Fig. 5(b), the temperature distribution of the double spiral energy pile is uniform. The temperature of the pile gradually increases from 24 ℃ to 53 ℃, which can reflect the influence of the heat transfer fluid on the pile temperature. The average transient heat exchange values per meter of single and double spiral energy piles are about 726.2 W/m and 746.2 W/m, and the energy utilization

rates are 94.4% and 97%, respectively. In summary, the heat transfer effect of the double spiral energy pile is better than that of the single one during heating. According to the data fitting analysis, in the natural cooling stage, the temperature of both piles decreases with time and eventually to the initial temperature.

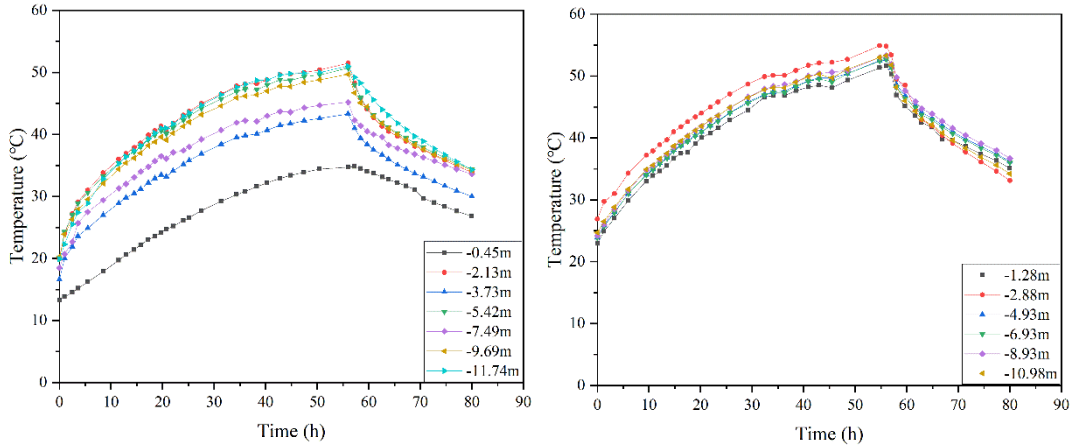

(a) Single spiral energy pile **(b) Double spiral energy pile**

Figure 5. Pile temperature variation with time

3.3. Pile strain variation

The state of force and deformation of energy piles under temperature and loading effects are related to the temperature variation, working load, and the restraining effect of the soil at the pile end and pile side. In this test, the steel bar stress was measured at different moments by embedding sensors on the main steel bar of the pile. Assuming that the vertical deformation of the pile is the same as that of the steel bar ($\varepsilon_P = \varepsilon_R$), the final pile strain can be obtained. The equation for the steel bar strain is as follows.

$$\varepsilon_P = \varepsilon_R = \frac{P_i}{A_s \times E_s} \tag{1}$$

where P_i is the force on the measured steel bar (kN); ε_R is the strain of the steel bar (με); ε_P is the strain of the pile (με); E_s is the elasticity modulus of the steel bar, with $E_s = 2 \times 10^5$ N/mm^2; A_s is the cross-sectional area of the single steel bar, with $A_s = 2.54 \times 10^{-4}$ m^2.

The strain curves at different depths and times are shown in Fig. 6. At the beginning of the test, the initial strain is not zero due to the pile top-loading effect. When the temperature of the pile body changes, the strain also changes. The energy pile thermally expands, and the pile strain at each depth shows a parabolic growth. The sensor at the top 1.28 m of the double spiral energy pile fails during natural cooling, but it does not impact the analysis of the results. At the end of heating, the minimum strain of the single spiral energy pile is 231 με at 11.74 m, and that of the double spiral energy pile is 216 με at 10.98 m. The two minimum strains appear near the pile bottom. The maximum strain of the single spiral energy pile is 347 με at 5.42 m, and that of the double spiral energy pile is 366 με at 4.93 m. The two maximum strains are all in the upper part of the pile.

The strain in the upper part of the pile is larger than that in the lower part because the restraint of the bearing stratum at the bottom of the pile is greater than that of the load at the top. Since the temperature of the double spiral energy pile at the end of heating is higher than that of the single spiral

energy pile, the pile strain is also higher than the strain of the single spiral energy pile. Overall, the strain at each end of the two piles during heating is less than that at other depths. During natural cooling, the strain changes in both piles tend to be identical. The decrease in temperature causes shrinkage deformation of the pile, and the strain decreases with time.

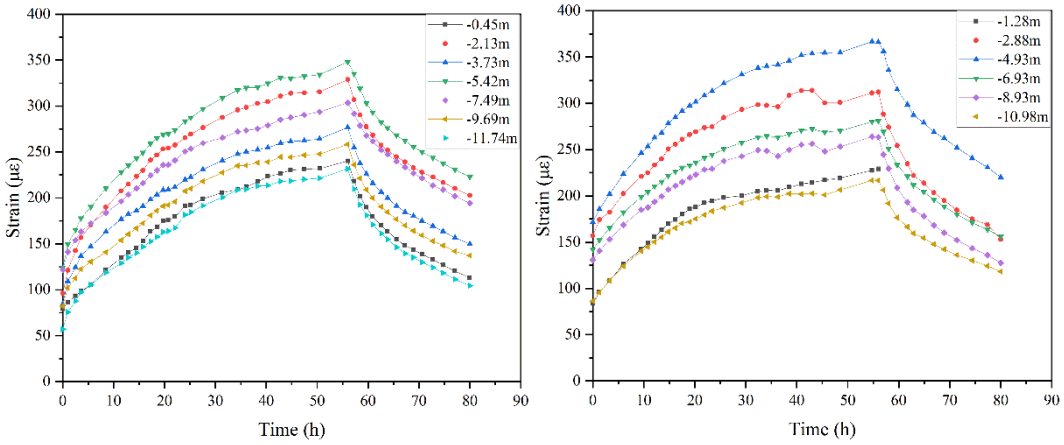

(a) Single spiral energy pile **(b) Double spiral energy pile**

Figure 6. The curve of the strain of piles with time

3.4. Pile axial force variation

The compressive stress of steel bar can be ignored when the deformation of steel bar and concrete is consistent. According to the measured force of steel bar and the elastic modulus of concrete, the pile axial force caused by temperature and loading can be calculated as Eq. (2).

$$T = E \times \frac{P_{\mathrm{i}}}{A_{\mathrm{s}} \times E_{\mathrm{s}}} \times A \tag{2}$$

where T is the axial force of the measured pile (kN); E is the elasticity modulus of concrete, with E = 3.25 × 10^4 N/mm^2; A is the pile cross-sectional area, with A = 0.5024 m^2. Other symbols mean the same as above. The axial force is positive when the pile thermally expands.

The axial force distribution during heating is shown in Fig. 7. At the beginning of heating, the thermal response of the two piles is obvious, and the axial force grows rapidly. In the middle and late stages of heating, the growth rate of the pile axial force decreases gradually because the temperature of the pile tends to stabilize. At the end of heating, the maximum axial force of the single spiral energy pile reaches 5681 kN at 5.42 m, and that of the double one reaches 5980 kN at 4.93 m. The additional compressive stresses caused by temperature changes during heating are 7.29 MPa and 6.33 MPa, which do not exceed the standard value of the compressive strength of concrete. The axial force of the single spiral energy pile decreases abruptly at 4 m, the junction of gravelly sand and fully weathered mudstone. The decrease is considered to be related to the different constraints of the bearing stratum at the location of the buried sensor.

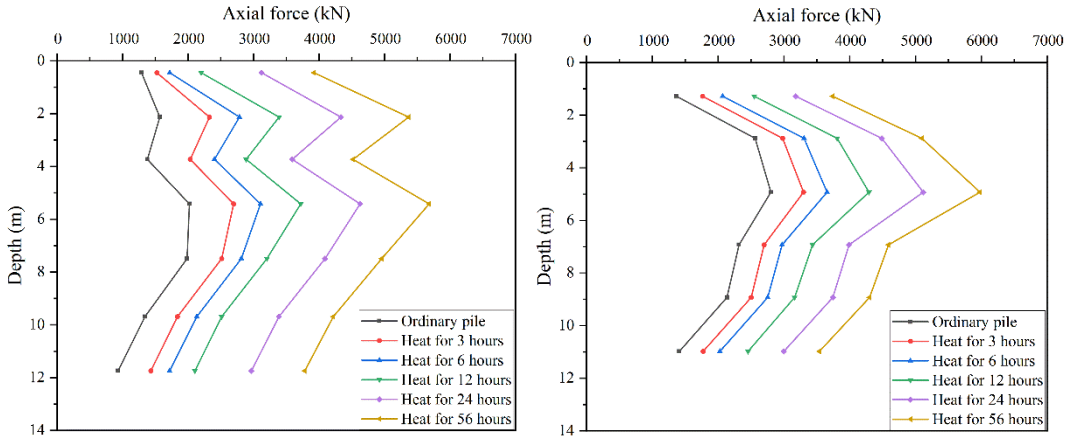

(a) Single spiral energy pile **(b) Double spiral energy pile**

Figure 7. Axial force distribution of piles during heating

In Fig. 8, the pile axial force shows an obvious downward trend. Cooling reduces the shrinkage deformation and the axial force of the pile. At the end of natural cooling, because the pile temperature has not returned to the initial temperature, the maximum axial forces of single and double spiral energy piles restore to 3640 kN and 3594 kN, respectively. The additional tensile stresses of single and double spiral energy piles generated during the cooling are 4.06 MPa and 4.75 MPa, which exceed the standard value of the concrete tensile strength. The above results show that the axial force of the energy pile changes significantly under the joint effect of temperature and loading. The two maximum axial forces are in the middle and upper half of the pile. Although the value does not exceed the ultimate design value of pile bearing capacity (the limit value of single pile bearing capacity in the test is 8400 kN), this axial force change may produce unrecoverable plastic deformation during continued loading and long-term temperature cycle, which should be fully considered in the design of the pile foundation structure.

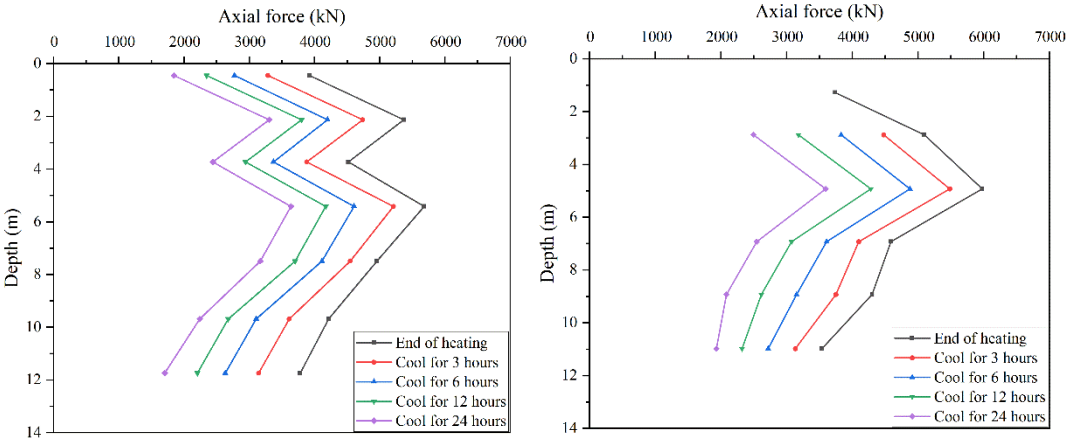

(a) Single spiral energy pile **(b) Double spiral energy pile**

Figure 8. Axial force distribution of piles during natural cooling

3.5. Distribution of pile shaft friction

Temperature fluctuations lead to changes in the additional stresses in the pile, causing changes in the pile shaft friction. The average shaft friction on the pile side between two adjacent monitoring sections can be calculated according to Eq. (3).

$$f_{s,\ mob,\ j} = (\sigma_{T,\ j} - \sigma_{T,\ j-1})\ D / 4\Delta L \tag{3}$$

Where $\sigma_{T,\ j}$ is the additional stress for each sensor buried layer (kPa); $f_{s,\ mob,\ j}$ is the average shaft friction of each sensor buried layer (kPa); D is the diameter of the pile (m); ΔL is the distance between two adjacent monitoring sections (m), and j = 1, 2, 3, 4, 5… indicates the buried layer number of the sensor. Pile shaft friction is positive upward and negative downward.

At the end of the test, the pile temperature does not drop to the initial temperature. Therefore, Fig. 9 only shows the change in pile shaft friction under heating. The pile is subjected to thermal expansion, and relative displacement occurs between the pile and the soil. The part above the neutral point moves upward relative to the soil, and the part below the neutral point moves downward relative to the soil. The pile shaft friction is negative in the middle and upper pile and positive in the middle and lower half. The pile shaft friction increases with the increase in pile temperature, but the increment decreases with time, indicating that the pile shaft friction gradually stabilizes with time. According to Fig. 9 (a), at the end of heating, the maximum positive shaft friction of the single spiral energy pile is 163 kPa within 5.42–7.49 m, and the maximum negative shaft friction is -276.6 kPa within 0.45–2.13 m. The resulting downward load is 1689 kN. The pile has two neutral points at 3.2 m and 4.5 m depth. As shown in Fig. 5 (a), because the top sensor is too close to the surface, the temperature change at this location of the pile during heating is less than that at other locations. The gravel layer below is thermally expanded and moves upward relative to the pile within 0–3.2 m depth and downward relative to the pile below the depth of 3.2 m, thus generating the neutral point.

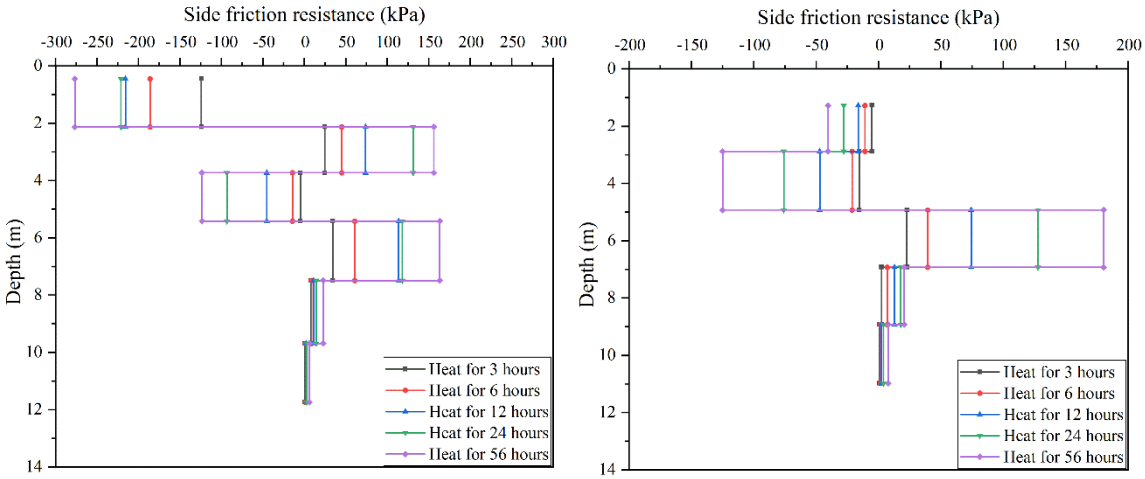

(a) Single spiral energy pile **(b) Double spiral energy pile**

Figure 9. Distribution diagram of pile shaft friction during heating

As shown in Fig. 9 (b), the maximum positive shaft friction of the double spiral energy pile at the end of heating is 180 kPa within 4.93–6.93 m, and the maximum negative shaft friction is -125 kPa within 2.88–4.93 m. The downward load considering the effect of negative shaft friction is 804 kN. The neutral point is located at 4.6 m depth. According to the changes in shaft friction of the two piles, the neutral point of both piles is found to be located above the middle of the pile. During heating, the temperature of the double spiral energy pile is higher than that of the single spiral energy pile; its temperature-induced shaft friction effect between the pile and the soil is higher; the change in shaft friction is greater. This is why the double spiral energy pile has higher maximum positive shaft friction

than the single spiral energy pile, which is also consistent with the axial force variation in the pile during heating. However, the temperature-induced downward load of the single spiral energy pile is increased by 885 kN compared with that of the double one. Hence, the settlement of the pile top caused by uneven temperature distribution of the single spiral energy pile may be intensified in the actual project of long-term operation. Related problems need attention.

4. Conclusions

Field tests of single and double spiral energy piles were conducted under the combined effect of temperature and loading, and the conclusions were obtained as follows.

During heating, the single spiral energy pile shows a discrete temperature distribution, while the double one does not. The heat exchange power of single and double spiral energy piles is stabilized at 9.44 kW and 9.7 kW, and the average transient heat exchange values of the piles per linear meter are about 726.2 W/m and 746.2 W/m, respectively. The total heat transfer and heat transfer efficiency of the double spiral energy pile is significantly higher than those of the single one.

The maximum strain of the pile lies in the upper part of the pile body during heating, while the minimum strain is at the end of the pile, basically showing a distribution law of small at both ends and large in the middle. The additional tensile stresses generated by the two energy piles during cooling reach -4.06 MPa and -4.75 MPa, exceeding the standard value of concrete tensile strength. Although the structural safety is not affected, the influence of the tensile stress changes generated by cooling on the bearing capacity of the piles cannot be ignored in the design process.

During heating, the shaft friction is negative in the middle and upper pile and positive in the middle and lower half. There are two neutral points in the single spiral energy pile. The single and double spiral energy piles produce downward loads of 1689 kN and 804 kN. The downward load caused by temperature in the single spiral energy pile is 885 kN higher than that in the double one. Therefore, in future practical projects, attention should be paid to the problems related to the aggravated settlement of the pile top caused by the uneven temperature distribution of single spiral energy piles.

Acknowledgment

This paper was made possible thanks to the generous support of the Education Department, Jilin Province (Grant No.:JJKH20220282KJ), the Science and Technology Department, Jilin Province (Grant No.: 20190303022SF).

[1] Liu, H. L., *et al*., Comparative model test on thermomechanical characteristics of energy pile with U-shape, W-shape and spiral-shape, *Rock and Soil Mechanics, 37* (2016), pp. 441-447 (in English)

[2] Lyu, W., *et al*., Thermal Performance of an Energy Pile Group with a Deeply Penetrating U-shaped Heat Exchanger, *Energies, 13* (2020), 5822

[3] Morino, K.; Oka, T., Study on heat exchanged in soil by circulating water in a steel pile, *Energy and Buildings, 21* (1994), pp. 65-78

[4] Yi, M., *et al*., A new model and analytical solutions for borehole and pile ground heat exchangers, *International Journal of Heat and Mass Transfer, 53* (2010), pp. 2593-2601

[5] Aks, A., *et al*., Pipe–pipe thermal interaction in a geothermal energy pile, *Geothermics, 81* (2019), pp. 209-223

[6] Wu, G., *et al*., Thermal Response Tests on PHC Energy Piles with Different Configuration of Heat Exchange Loop, *Journal of Disaster Prevention and Mitigation Engineering, 39* (2019), pp. 615-621

[7] Lu, C., *et al*., Field tests on thermal-mechanical coupling characteristics of energy pile in pile-raft foundation, *Rock and Soil Mechanics, 40* (2019), pp. 3569-3575 (in English)

[8] Lv, Z., *et al*., Effects of Soil Type on Axial and Radial Thermal Responses of Field-Scale Energy Piles, *Journal of Geotechnical and Geoenvironmental Engineering, 146* (2020), 06020018

[9] Du, T., *et al*., Thermo-Mechanical Performance of a Phase Change Energy Pile in Saturated Sand, *Symmetry, 12* (2020), 1781

[10] Chang, H.; Jin, L., Preparation and Heat Transfer Performance of Steel Ball Phase Change Concrete, *Journal of New Materials for Electrochemical Systems, 23* (2020), pp. 204-212

[11] Sliwa, T., *et al*., Strength Tests of Hardened Cement Slurries for Energy Piles, with the Addition of Graphite and Graphene, in Terms of Increasing the Heat Transfer Efficiency, *Energies, 14* (2021), 1190

[12] Liu, H. L., *et al*., Ultimate bearing capacity of energy piles in dry and saturated sand, *Acta Geotechnica, 14* (2018), pp. 869-879

[13] Yazdani, S., *et al*., Investigation of thermal loading effects on the shaft resistance of energy pile using laboratory scale model, *Journal of Geotechnical and Geoenvironmental Engineering, 145* (2019), 04019043

[14] Zhu, W. L., *et al*., Model test on bearing capacity characteristics of energy piles in saturated clay, *IOP Conference Series: Earth and Environmental Science, 787* (2021), 012157

[15] Liao, Z., *et al*., A novel 2-D equivalent numerical model of helix energy pile based on heat transfer characteristics of internal heat convection, *Geothermics, 95* (2021), 102150

[16] Garbellini, C.; Laloui, L., Three-dimensional finite element analysis of piled rafts with energy piles, *Computers and Geotechnics, 114* (2019), 103115

[17] Yoon, S., *et al*., Evaluation of thermal efficiency in different types of horizontal ground heat exchangers, *Energy and Buildings, 105* (2015), pp. 100-105

[18] Park, S., *et al*., Relative constructability and thermal performance of cast-in-place concrete energy pile: Coil-type GHEX (ground heat exchanger), *Energy, 81* (2015), pp. 56-66

[19] You, T., *et al*., Soil thermal imbalance of ground source heat pump systems with spiral-coil energy pile groups under seepage conditions and various influential factors, *Energy Conversion and Management, 178* (2018), pp. 123-136

[20] Ministry of Construction of the People's Republic of China., *Code for Design of Concrete Structures*, China Architecture&Building Press., Beijing, China, 2011 (in English)

Submitted: 07.03.2022

Revised: 20.07.2022

Accepted: 26.07.2022